PROCEEDINGS A

rspa.royalsocietypublishing.org

Research

Cite this article: Gao T, Wang Z, Vanden-Broeck J-M. 2016 On asymmetric generalized solitary gravity–capillary waves in finite depth. *Proc. R. Soc. A* **472**: 20160454. http://dx.doi.org/10.1098/rspa.2016.0454

Received: 6 June 2016
Accepted: 12 September 2016

Subject Areas:
fluid mechanics, wave motion

Keywords:
generalized solitary waves, asymmetric waves, gravity–capillary waves

Author for correspondence:
Z. Wang
e-mail: z.wang5@bath.ac.uk

On asymmetric generalized solitary gravity–capillary waves in finite depth

T. Gao[1], Z. Wang[2,3] and J.-M. Vanden-Broeck[1]

[1]Department of Mathematics, University College London, London WC1E 6BT, UK
[2]Key Laboratory for Mechanics in Fluid Solid Coupling Systems, Institute of Mechanics, Chinese Academy of Sciences, Beijing 100190, People's Republic of China
[3]School of Engineering Science, University of Chinese Academy of Sciences, Beijing 100049, People's Republic of China

ZW, 0000-0003-4393-2118

Generalized solitary waves propagating at the surface of a fluid of finite depth are considered. The fluid is assumed to be inviscid and incompressible and the flow to be irrotational. Both the effects of gravity and surface tension are included. It is shown that in addition to the classical symmetric waves, there are new asymmetric solutions. These new branches of solutions bifurcate from the branches of symmetric waves. The detailed bifurcation diagrams as well as typical wave profiles are presented.

1. Introduction

Progressive waves propagating at the surface of a fluid of finite depth have been studied intensively over the years. It is usually assumed that the fluid is inviscid and incompressible and that the flow is irrotational. Different types of nonlinear solutions, such as periodic waves, solitary waves, dark solitary waves, and generalized solitary waves, were identified (see e.g. [1,2] and references therein). In this paper, we focus on the generalized solitary waves. Such waves are characterized by a solitary pulse with non-decaying ripples in the far field.

When gravity and surface tension are both taken into account, the solution structure depends on the value of the Bond number

$$B = \frac{T}{\rho g H^2}, \tag{1.1}$$

THE ROYAL SOCIETY PUBLISHING

where T is the surface tension, ρ is the density, g is the acceleration of gravity and H is the undisturbed depth of the fluid. When $B > 1/3$, long waves of small amplitude satisfy the Korteweg–de Vries (KdV) equation. The solutions are then depression solitons. The existence of KdV-type solitary waves for the full Euler equations was rigorously proved by Amick & Kirchgässner [3]. However, the KdV equation is no longer the correct simplified model when $0 < B < 1/3$, and many different families of solutions, including solitary waves and generalized solitary waves are then possible (see, for example, the numerical work [4]). The mathematical proof of the existence of elevation generalized solitary waves was provided by Beale [5] and Sun [6]. Later, Champneys *et al*. [7] showed that the amplitude of the ripples in the far field is always different from zero. More recently, Clamond *et al*. [8] found new multi-hump generalized solitary waves and the numerical results suggest that the existence of an infinite number of such waves.

The works mentioned in the previous paragraphs are restricted to symmetric waves, i.e. waves whose profiles are symmetric with respect to some vertical axis. Asymmetric gravity–capillary waves were first studied by Zufiria [9] based on an analysis of the fifth-order KdV equation (a reduced model for small-amplitude waves when the Bond number is close to 1/3). Zufiria found numerically asymmetric periodic waves with six peaks in one wavelength. This problem was further explored by Shimizu & Shōji [10], who found both 6-peak and 2-peak asymmetric solutions for the full Euler equations in deep water. New results in [11] suggest that asymmetric periodic gravity–capillary waves exist in the form of any number (no less than 2) of peaks in one wavelength. Zufiria's work [9] also showed that asymmetric solitary waves are possible for the fifth-order KdV equation. Using exponential asymptotics for the same reduced model, Yang & Akylas [12] showed that asymmetric solitary waves feature a multi-packet structure. Recently, Wang *et al*. [13] discovered numerically the counterparts in deep water for the Euler equations. However, to the best of our knowledge, asymmetric generalized solitary waves have not been found for water waves. In this paper, we provide a first numerical evidence for the existence of these solutions in the full Euler equations.

In the remaining part of the paper, we restrict our attention to $0 < B < 1/3$ and search for asymmetric generalized solitary gravity–capillary waves. The formulation and the numerical method are described in §2. The numerical results are presented in §3. Finally, some concluding remarks are given in §4.

2. Formulation and numerical method

We consider an irrotational flow of a two-dimensional, inviscid and incompressible fluid bounded below by a flat bottom. The upper surface of the fluid is deformed by a train of waves travelling at a constant velocity c. A frame of reference moving with the waves is used so that the flow is steady. We introduce Cartesian coordinates with the y-axis pointing upwards. A schematic of the flow configuration is presented in figure 1. We denote the complex velocity potential by $f = \phi + \mathrm{i}\psi$, where ϕ is a potential function and ψ is the streamfunction. We choose $\psi = 0$ on the free surface and $\phi = 0$ at a crest or a trough of the wave where we assume that $x = y = 0$. We denote by $\psi = -Q$ the value of the streamfunction on the bottom. The equation of the free surface is given by $y = \eta(x)$. We shall approximate the generalized solitary waves by periodic waves of very long wavelength λ. Next we define also the wave amplitude

$$A = \eta\left(\frac{\lambda}{2}\right). \tag{2.1}$$

The governing equations can be written as

$$\nabla^2\phi = 0, \qquad -H < y < \eta(x), \tag{2.2}$$

$$\phi_y = \phi_x\eta_x, \qquad \text{on } y = \eta(x), \tag{2.3}$$

$$\frac{1}{2}|\nabla\phi|^2 + gy - \frac{T}{\rho}\kappa = B_0, \quad \text{on } y = \eta(x) \tag{2.4}$$

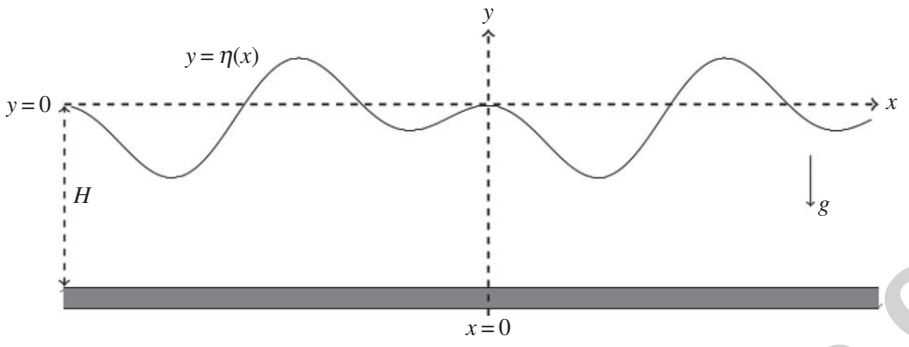

Figure 1. Configuration of the problem. The gravity acts in the negative y-direction. We denote the unknown free surface by $y = \eta(x)$. We choose the origin to be at a wave crest or trough.

and
$$\phi_y = 0, \qquad \text{on } y = -H, \tag{2.5}$$

where κ is the curvature of the free surface and B_0 is the Bernoulli constant. Equations (2.3) and (2.5) are the kinematic boundary conditions on the free surface and on the bottom, respectively. Equation (2.4) is the dynamic boundary condition.

We use ϕ and ψ as independent variables. Next we introduce the complex velocity $w = u - \mathrm{i}v$ and define the function $\mathcal{T} - \mathrm{i}\vartheta$ by

$$u - \mathrm{i}v = \exp(\mathcal{T} - \mathrm{i}\vartheta). \tag{2.6}$$

Here, u and v are the horizontal and vertical components of the vector velocity, respectively.

The kinematic boundary condition (2.5) on the bottom can be automatically satisfied by using the method of images. The image of the free-surface into the bottom is then $\psi = -2Q$. Hence the extended flow domain in the complex f-plane is the strip $-2Q < \psi < 0$. Next we introduce the conformal mapping

$$s = \exp\left(-\frac{2\mathrm{i}\pi f}{c\lambda}\right), \tag{2.7}$$

which maps the strip onto the annulus $r_0^2 < |s| < 1$. Here

$$r_0 = \exp\left(\frac{-2\pi Q}{c\lambda}\right), \tag{2.8}$$

and c is the speed of the wave defined as

$$c = \frac{1}{\lambda}\int_0^\lambda \phi_x \,\mathrm{d}x, \tag{2.9}$$

where the integral is evaluated at a level $y = \text{const.}$ in the fluid. The function $\mathcal{T} - \mathrm{i}\vartheta$ can be viewed as an analytic function of s in the annulus $r_0^2 < |s| < 1$. Therefore, it can be represented by the Laurent series

$$\mathcal{T} - \mathrm{i}\vartheta = a_0 + \sum_{n=1}^{\infty} \alpha_n s^n + \sum_{n=1}^{\infty} \beta_n s^{-n}. \tag{2.10}$$

Imposing the condition that $\psi = -2Q$ is the image of the free surface $\psi = 0$ yields the relation

$$\beta_n = \alpha_n r_0^{2n}. \tag{2.11}$$

Therefore, (2.10) can be rewritten as

$$\mathcal{T} - \mathrm{i}\vartheta = a_0 + \sum_{n=1}^{\infty} \alpha_n s^n + \sum_{n=1}^{\infty} \alpha_n r_0^{2n} s^{-n}. \tag{2.12}$$

We now introduce dimensionless variables by using H as the reference length and c as the reference velocity. The dynamic boundary condition (2.4) becomes

$$\frac{F^2}{2}\,\mathrm{e}^{2\mathcal{T}} + y - B\kappa = \tilde{B}_0, \tag{2.13}$$

where $\tilde{B}_0 = B_0 F^2$ is unknown, B is the Bond number defined by (1.1) and

$$F = \frac{c}{\sqrt{gH}} \tag{2.14}$$

is the Froude number. The other governing equations remain unchanged. The coefficients α_n are in general complex. Therefore, we write

$$\alpha_n = a_n + \mathrm{i}b_n \tag{2.15}$$

and find a_n and b_n numerically. First, we truncate the infinite series in (2.12) after N terms and define the $2N+1$ collocation points

$$\phi_I = \left(\frac{j-1}{N} - 1\right)\frac{\lambda}{2}, \quad j = 1, 2, \ldots, 2N+1, \tag{2.16}$$

where λ is now the dimensionless wavelength. The dynamic boundary condition (2.13) is then satisfied at the points (2.16). This yields a system of $2N+1$ equations. We also note that (2.9) implies the equation

$$x\left(\frac{\lambda}{2}\right) - x\left(\frac{-\lambda}{2}\right) = \lambda. \tag{2.17}$$

The final equation is obtained by writing

$$A = \tilde{A} \tag{2.18}$$

or

$$b_m = \epsilon, \tag{2.19}$$

where $\tilde{A}$ and ϵ are given parameters and m is an integer suitably chosen. We note that (2.18) is useful for computing symmetric waves and that (2.19) is useful for asymmetric waves. The two additional equations (2.17), (2.18) or (2.19) together with the $2N+1$ equations obtained earlier form a system of $2N+3$ equations with $2N+3$ unknowns $(a_0, a_1, \ldots, a_N, b_1, b_2, \ldots, b_N, F, \tilde{B}_0)$. Finally, to avoid the Galilean invariance of the Euler equations, we replace one of the algebraic equations resulting from the discretization of the Bernoulli equation by

$$\sum_{n=1}^{N} (1 + r_0^{2n}) b_n = 0. \tag{2.20}$$

This condition is used to make sure that a crest or a trough lies at the origin. The method was first proposed by Shimizu [10] and followed by Gao *et al*. [11] in searching for asymmetric surface water waves. Then the system can be solved by Newton's method for given values of B and λ. We refer to this system as the asymmetric system.

We now consider the case of symmetric waves. As mentioned in §1, these waves have profiles which are symmetric with respect to some vertical line. Without loss of generality, we choose this line of symmetry to coincide with the y-axis. It follows that all the coefficients b_n are zero. The code can then be simplified by taking $N+1$ equally spaced collocation points uniformly distributed along $[0, \lambda/2]$. We then have a system of $N+3$ nonlinear equations for the $N+3$ unknowns $(a_0, a_1, \ldots, a_N, F, \tilde{B}_0)$ (e.g. [14]). We refer to this system as the symmetric system.

The basic idea of our computations is first to write the symmetric solutions in the form of $(a_0, a_1, \ldots, a_N, 0, 0, \ldots, 0, F, \tilde{B}_0)$, then to show that there are bifurcation points on the branches of symmetric waves. This is achieved by monitoring the sign of the Jacobian of the asymmetric system and identifying points where the Jacobian vanishes. To ease referring, we call this operation the *asymmetric Jacobian test*. We found that new branches of asymmetric solutions bifurcate from the branches of symmetric solutions at these points. We usually take $N = 800$

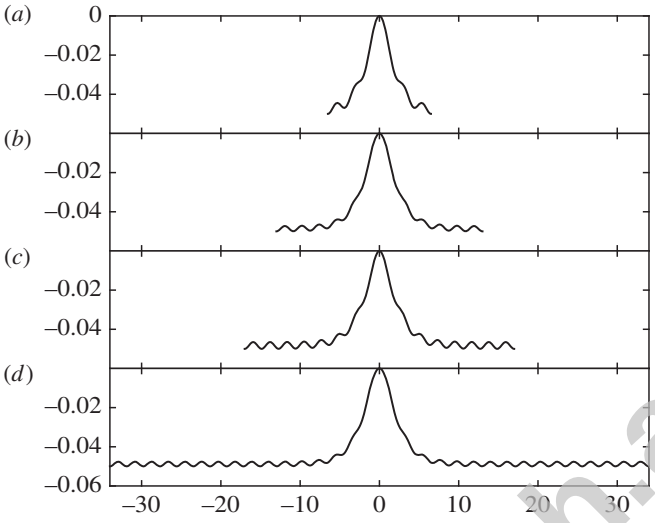

Figure 2. Profiles of the waves for $A = -0.05$, $B = 0.24$ and (*a*) $\lambda = 13$, (*b*) $\lambda = 26$, (*c*) $\lambda = 34$ and (*d*) $\lambda = 68$. The corresponding values of the Froude number are (*a*) 0.999, (*b*) 1.011, (*c*) 1.014 and (*d*) 1.020.

for computing symmetric waves and $N = 1600$ for asymmetric waves. The residual l^∞-norm error is set to be less than 10^{-9} in Newton's method. This numerical scheme was successfully implemented in [11,14,15], and its convergence and accuracy were carefully validated in [14].

As mentioned earlier, we shall approximate the generalized solitary waves by periodic waves of long wavelength. These families of solutions are then characterized by three parameters which can be, for example, chosen as A, B and λ. The search for the bifurcation points would be very complicated if we let all the parameters vary at the same time. For simplicity, we choose to fix the value of two of the parameters and to study the branches of solutions in a two-dimensional space. We then perform the *asymmetric Jacobian test* to locate the bifurcation points which lead to symmetry breakings. We also show that our approach uncovers the existence of new symmetric solutions.

3. Numerical results

The size of the computational domain λ has to be chosen carefully in order to compute accurately generalized solitary waves [4,8,14]. This is illustrated in figure 2 where we present symmetric waves for $B = 0.24$, $A = -0.05$ and various values of λ. As the wavelength increases, the periodic solutions approach the configuration of a solitary pulse in the middle with small ripples in the tails. The profile in figure 2*d* can then be viewed as a good approximation of a generalized solitary wave (i.e. a non-periodic wave with train of ripples extending up to $|x| = \infty$). In all the calculations presented in this paper, we chose $\lambda = 102$. This value was found to be sufficiently large to model symmetric and asymmetric generalized solitary waves. It is worth mentioning that there are two types of periodic waves as shown in figure 3. The wave (*a*) and (*b*) have a trough and a crest, respectively, at their right-endpoint. However, these two types of waves approach the same generalized solitary wave as $\lambda \to \infty$. In this paper, we only focus on the families of solutions ending with a crest since the results for those ending with a trough are expected to be similar.

We fix the value of A (here $A = -0.055$) and compute the branch of symmetric solutions by using the numerical scheme described in §2. The results in the F^2–B plane are shown in figure 4 (solid curve). Since there are many turning points on the bifurcation curve, we need to use in addition to the code of §2 a variant in which we fix F and λ and take $(a_0, a_1, \ldots, a_N, B, \tilde{B}_0)$ as the unknowns. The solid curve of figure 4 was then obtained by using alternatively both codes

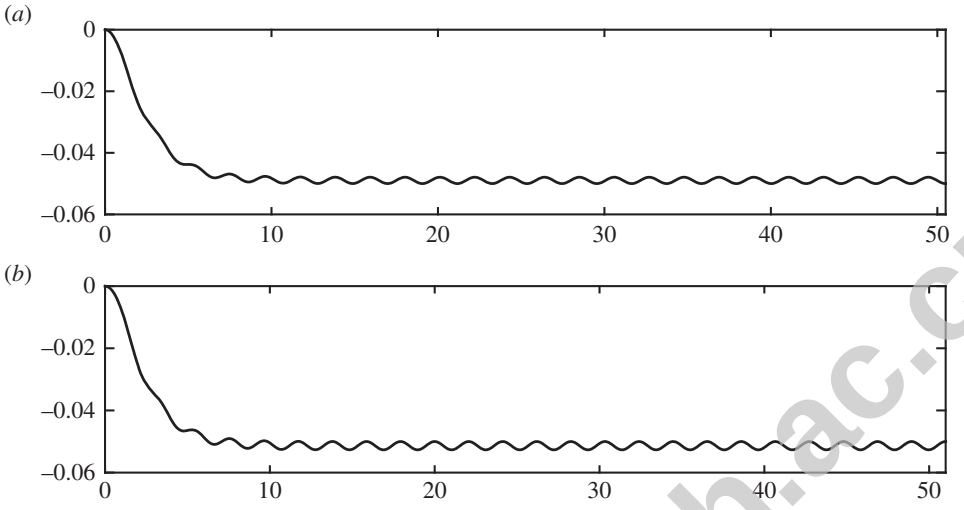

Figure 3. Typical free-surface profiles of generalized solitary waves with (*a*) $F = 1.021$, $B = 0.239$, $\lambda = 101$ and (*b*) $F = 1.023$, $B = 0.239$ and $\lambda = 102$. The waves (*a*, *b*) end with a trough and a crest, respectively. Only half of the waves are shown.

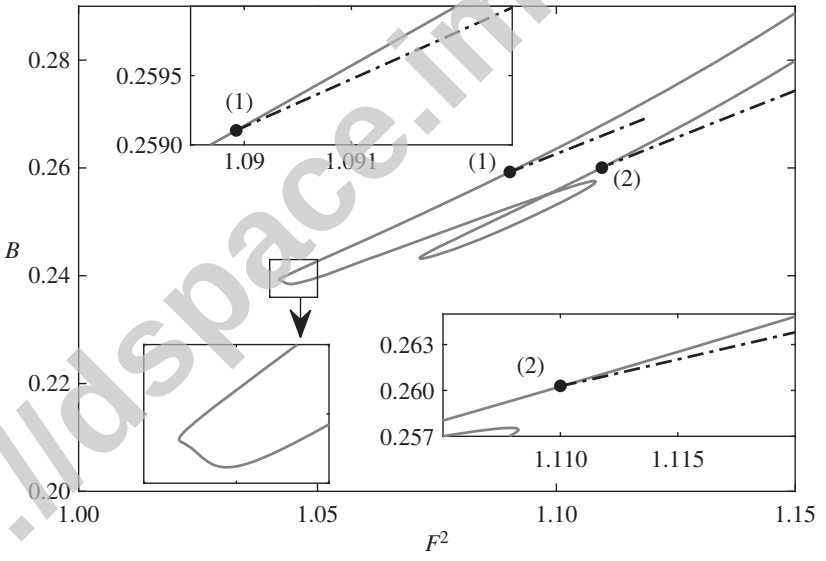

Figure 4. Bifurcation diagram plotted in the F^2–B plane with $A = -0.055$ and $\lambda = 102$. The solid curve is the branch of symmetric waves. The two dashed-dotted curves are the branches of asymmetric waves bifurcating at (1) $F = 1.044$, $B = 0.259$ and (2) $F = 1.054$, $B = 0.261$, respectively. The corresponding wave profiles are presented in figure 5.

and continuation (i.e. using a previously computed solution as an initial guess to compute a new solution for slightly different values of the parameters). By performing the *asymmetric Jacobian test*, we located two bifurcation points (marked as (1) and (2) in figure 4) from which new asymmetric branches emanate. Typical wave profiles are shown in figure 5. As can be seen from (1†), (2†), (1‡) and (2‡), there are asymmetries in the middle of the profile while the ripples in the far field are still of equal amplitude.

We then continued to search for more asymmetric generalized solitary waves. We first used the solution (2) in figure 4 and constructed by continuation a branch of symmetric solutions for

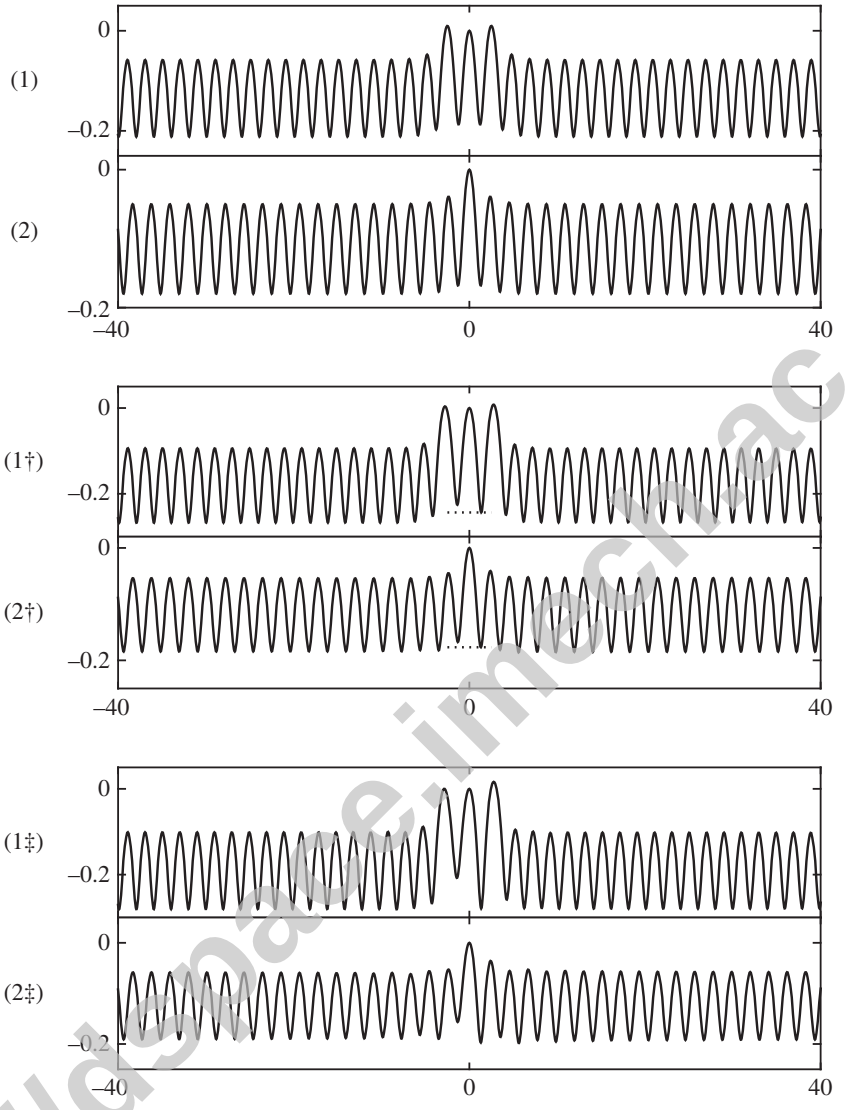

Figure 5. Figures (1) and (2) are the wave profiles corresponding to the points (1) and (2) of figure 4. Figures (1†, 1‡) and (2†, 2‡) are typical wave profiles of asymmetric generalized solitary waves taken, respectively, on the branches bifurcating from the points (1) and (2) of figure 4. The profiles of figures (1†) and (2†) correspond to points close to the bifurcation points (1) and (2). The horizontal dashed lines illustrate clearly the asymmetry. The profiles of figures (1‡) and (2‡) correspond to the points further away from the bifurcation points. All the profiles are plotted in the physical plane, and only the central parts are shown.

$B = 0.26$ and $\lambda = 102$. This branch is shown in the F^2–A plane of figure 6. Next we chose a point on the curve of figure 6 (here we chose the point (*d*)) and constructed a family of symmetric waves by fixing $A = -0.0935$ and $\lambda = 102$. It is shown by the solid curve in the F^2–B plane of figure 7. As we did previously in figure 4, we perform the *asymmetric Jacobian test*. This enabled us to identify a bifurcation point (the point (3)) from which a branch of asymmetric waves emanated (see dashed curve in figure 7). Typical wave profiles are shown in figure 8. It turns out that the far field is deformed by a train of Wilton-ripple-like tails in (3†) instead of simple ripples of constant amplitude. Generalized solitary waves with Wilton-ripple-like trains were first found by Wang *et al*. [16] for interfacial waves under an elastic sheet. For the classical gravity–capillary waves, such kind of solutions had not been found before to our knowledge.

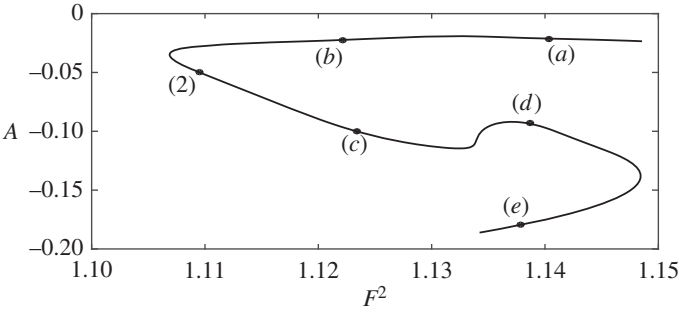

Figure 6. A branch of symmetric waves plotted in the F^2–A plane when we fix $B = 0.26$ and $\lambda = 102$.

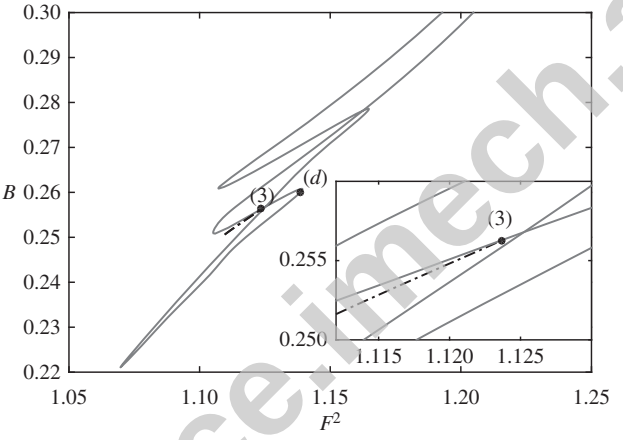

Figure 7. A family of symmetric solutions plotted in the F^2–B plane when $A = -0.0935$ and $\lambda = 102$. This branch emanates from the point (d) of figure 6. A symmetry-breaking point is found at $F = 1.124$, $B = 0.256$ and marked as (3) in the graph. The branch of asymmetric waves is shown by the dash-dotted curve. The zoom-in figure is used to differentiate the bifurcation point (3) and the intersection point.

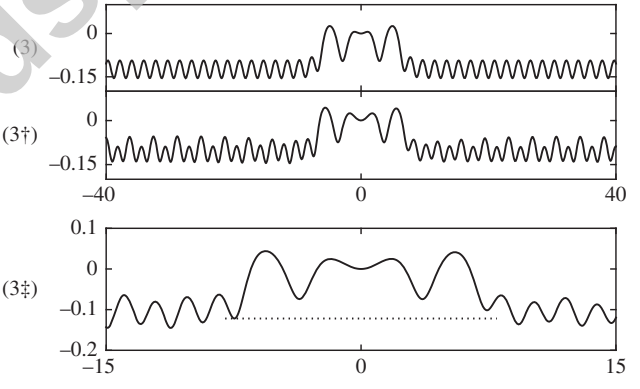

Figure 8. Wave profile (3) for the point spotted in figure 7. (3†) is a typical profile of asymmetric generalized solitary waves which bifurcate from (3) and (3‡) is the blow-up graph of (3†). The profiles are plotted in the physical plane, and only the main profiles are shown.

Our aim in this paper was to demonstrate the existence of branches of asymmetric generalized solitary waves. As part of our search we found some new symmetric waves. We shall conclude this section by presenting some typical profiles. These symmetric results supplement those obtained in [8]. First we show in figure 9 wave profiles corresponding to the points (a–e) of

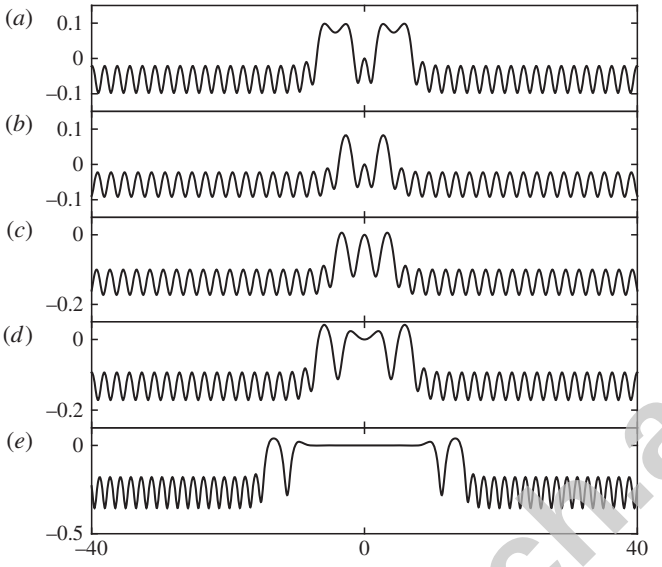

Figure 9. Wave profiles for the points indicated in figure 6. All the profiles are plotted in the physical plane, and only the essential parts of the waves are shown.

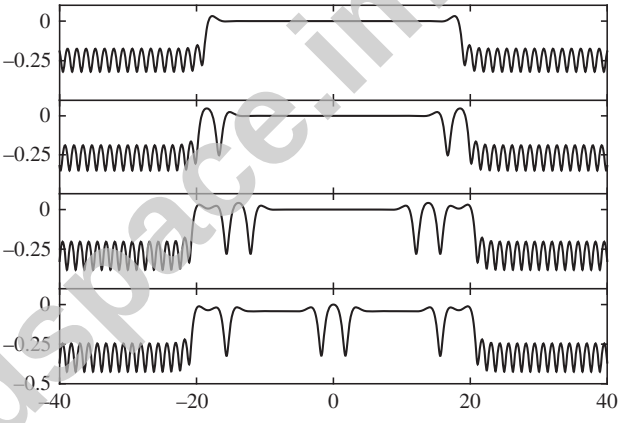

Figure 10. A few extra symmetric wave profiles. All the profiles are plotted in the physical plane, and only the main profiles are shown.

figure 6. At one end of the solution branch, multi-hump solutions have been found as presented in figure 9*a*. At the other end, we observed a new kind of generalized solitary wave with a large and long ripple in the middle. We followed to use this solution (*e*) as an initial guess to seek more new solutions. The resulting profiles are presented in figure 10 which show that the large and long central ripple can evolve multiple ripples. It is noted that there is a plethora of multi-hump generalized solitary gravity–capillary waves as claimed in [8,17].

4. Conclusion

We have revisited the classical problem of generalized solitary waves in the presence of gravity and surface tension. We have shown numerically the existence of new asymmetric solutions. These solutions form branches which bifurcate from the classical branches of symmetric generalized solitary waves. Since the branches are characterized by three parameters, we could only present a few typical results which demonstrate clearly the existence of asymmetric waves.

Ethics. This work did not involve any active collection of human data, but only computer simulations of human behavior.

Authors' contributions. T.G., Z.W. and J.M.V.B. conceived the mathematical models, interpreted the numerical results and wrote the paper. T.G. implemented and performed most of the computations with Z.W. and J.M.V.B. All authors gave final approval for publication.

Competing interests. We have no competing interests.

Funding. This work was supported by National Natural Science Foundation of China (grant no. 11232012) and Key Research Program of Frontier Sciences, CAS (grant no. QYZDB-SSW-SYS015).

References

1. Dias F, Kharif C. 1999 Nonlinear gravity and capillary-gravity waves. *Annu. Rev. Fluid Mech.* **31**, 301–346. (doi:10.1146/annurev.fluid.31.1.301)
2. Vanden-Broeck JM. 2010 *Gravity-capillary free-surface flows*. Cambridge, UK: Cambridge University Press.
3. Amick CJ, Kirchgässner K. 1989 A theory of solitary water-waves in the presence of surface tension. *Arch. Rat. Mech. Anal.* **105**, 1–49. (doi:10.1007/BF00251596)
4. Hunter JK, Vanden-Broeck JM. 1983 Solitary and periodic gravity-capillary waves of finite amplitude. *J. Fluid Mech.* **134**, 205–219. (doi:10.1017/S0022112083003316)
5. Beale JT. 1991 Exact solitary water waves with capillary ripples at infinity. *Comm. Pure Appl. Math.* **44**, 211–257. (doi:10.1002/cpa.3160440204)
6. Sun SM. 1991 Existence of a generalized solitary wave solution for water with positive Bond number less than $\frac{1}{3}$. *J. Math. Anal. Appl.* **156**, 471–504. (doi:10.1016/0022-247X(91)90410-2)
7. Champneys AR, Vanden-Broeck J-M, Lord GJ. 2002 Do true elevation gravity-capillary solitary waves exist? A numerical investigation. *J. Fluid Mech.* **454**, 403–417. (doi:10.1017/S0022112001007200)
8. Clamond D, Dutykh D, Durán A. 2015 A plethora of generalised solitary gravity-capillary water waves. *J. Fluid Mech.* **784**, 664–680. (doi:10.1017/jfm.2015.616)
9. Zufiria JA. 1987 Symmetry breaking in periodic and solitary gravity-capillary waves on water of finite depth. *J. Fluid Mech.* **184**, 183–206. (doi:10.1017/S0022112087002854)
10. Shimizu C. 2012 Appearance and disappearance of non-symmetric progressive capillary-gravity waves of deep water. *Jpn J. Indust. Appl. Math.* **29**, 331–353. (doi:10.1007/s13160-012-0070-4)
11. Gao T, Wang Z, Vanden-Broeck JM. Submitted. Investigation of symmetry-breaking in gravity-capillary waves. *J. Fluid Mech.*
12. Yang TS, Akylas TR. 1997 On asymmetric gravity-capillary solitary waves. *J. Fluid Mech.* **330**, 215–232. (doi:10.1017/S0022112096003643)
13. Wang Z, Vanden-Broeck JM, Milewski PA. 2014 Asymmetric gravity-capillary solitary waves on deep water. *J. Fluid Mech.* **759**, R2. (doi:10.1017/jfm.2014.567)
14. Gao T, Vanden-Broeck JM. 2014 Numerical studies of two-dimensional hydroelastic periodic and generalised solitary waves. *Phys. Fluids* **26**, 087101. (doi:10.1063/1.4893677)
15. Vanden-Broeck JM. 1996 Capillary waves with variable surface tension. *Z. Angew. Math. Phys.* **47**, 799–808. (doi:10.1007/BF00915276)
16. Wang Z, Părău EI, Milewski PA, Vanden-Broeck JM. 2014 Numerical study of interfacial solitary waves propagating under an elastic sheet. *Proc. R. Soc. A* **470**, 20140111. (doi:10.1098/rspa.2014.0111)
17. Buffoni B, Champneys AR, Toland JF. 1996 Bifurcation and coalescence of a plethora of homoclinic orbits for a Hamiltonian system. *J. Dyn. Differ. Equ.* **8**, 221–279. (doi:10.1007/BF02218892)